

# **Coastal Ocean Response to Extratropical Storms in March 2001: A Retrospective Analysis using Sub-Regional Coastal Ocean Models of the Southeast Atlantic Coastal Ocean Observing System (SEACOOS)**

Ruoying He<sup>1\*</sup>, Inkweon Bang<sup>2</sup>, Karen P. Edwards<sup>3</sup>,  
Christopher N.K. Mooers<sup>2</sup>, Robert H. Weisberg<sup>4</sup>, Francisco Werner<sup>3</sup>

Woods Hole Oceanographic Institution <sup>1</sup>  
University of Miami <sup>2</sup>  
University of North Carolina, Chapel Hill <sup>3</sup>  
University of South Florida <sup>4</sup>

Submitted to the Journal of Atmospheric and Oceanic Technology

May, 2005

---

Corresponding author. Tel: 1-508-289-3671; Fax: 1-508-289-2491;  
Email: [rhe@who.edu](mailto:rhe@who.edu) (Ruoying He)  
Mail stop 10, Woods Hole Oceanographic Institution  
Woods Hole, MA 02543

## Abstract

The responses of the U.S. southeast coastal ocean to extratropical storm passages in March 2001 are considered from the perspective of the regional observations and models comprising the Southeast Atlantic Coastal Ocean Observing System (SEACOOS). SEACOOS is a prospective element of the emergent national network of coastal ocean observing systems. It is intended to inclusively cover the coastal ocean (i.e., Exclusive Economic Zone) off the states of North Carolina, South Carolina, Georgia, and Florida. SEACOOS coastal ocean circulation modeling is focused on three sub-regional models (with overlapping domains). Each of these sub-regional models employs a three-dimensional, free-surface, primitive equation formulation with a higher order turbulence closure, to simulate the tidal and sub-tidal variability of the currents and sea surface heights in response to external forcing. Here, the performance of these sub-regional models in hindcasting the coastal ocean responses to two intense extratropical storm passages during March 2001 is evaluated. The model solutions are tested under three scenarios to examine the effects of tidal friction and stratification in their respective sub-domains. Comparisons between model hindcasts and *in-situ* observations are made to evaluate each sub-regional model's performance. Maps of misfits between adjacent sub-regional model products are assessed.

## 1. Introduction

The coastal ocean of the southeast United States (U.S.) contains adjoining continental shelves of varying widths (Fig. 1), being mainly broad on the West Florida Shelf [WFS] (100-150 km), narrow on the Southeast Florida Shelf (1-10 km) and gradually broadening and then narrowing in the South Atlantic Bight [SAB] (30-100 km). Here, the East Florida Shelf (EFS) sub-region covers the Southeast Florida Shelf and the southern third of the SAB; i.e., the Northeast Florida Shelf; and the Carolina-Georgia Bight (CGB) sub-region covers the northern two thirds of the SAB. Because of its geographic location, the southeast U.S. experiences easterly waves (*Gu and Zhang, 2002*) and tropical cyclone passages in summer, and extratropical cyclone (e.g. Nor'easters) and cold front passages in winter (*Weisberg and Pietrafesa, 1983; Bane, et al., 1989; Blanton et al., 1989; Lee et al., 1989, Peng et al., 1999*). Such synoptic scale atmospheric disturbances over the CGB, EFS, and WFS sub-regions induce strong physical

responses in the coastal ocean, including changes in sea level, across shelf and along shelf currents, coastal upwelling and downwelling, subtidal coastally-trapped waves (*Brooks and Mooers, 1977a and 1977b*), stratification, surface waves, and turbulent mixing. These responses to weather forcing often have significant socioeconomic effects through storm surges, rip currents, beach erosion, coastal upwelling/downwelling, nutrient transport, and related primary productivity including harmful algal blooms.

Due to the complexity of the coastal ocean, monitoring and predicting coastal ocean processes such as the aforementioned require a coastal ocean observing system that can incorporate both extensive *in-situ* (and satellite and coastal remote sensing ) observations and numerical models. One such initiative is the Southeast Atlantic Coastal Ocean Observing System (SEACOOS), a partnership among the University of North Carolina-Chapel Hill (UNC), University of South Carolina (USC), Skidaway Institution of Oceanography (SkIO), University of Miami (UM), and University of South Florida (USF), that inclusively covers the coastal ocean off North Carolina, South Carolina, Georgia, and Florida. All partners have sustained observing programs; UNC, UM, and USF additionally run sub-regional ocean circulation models in a continual, automated fashion (i.e., quasi-operationally) and make an integrated product of surface fields (<http://seacoos.org>). A SEACOOS goal is to achieve coherent descriptions and accurate predictions of the state and evolution of the coastal ocean environment through the integration of observations and models, and to provide them for societal and scientific applications.

The starting point for SEACOOS circulation modeling is the set of sub-regional models existing at UNC, UM, and USF, each being a three-dimensional, free-surface, primitive equation model, with a higher order turbulence closure, to study the tidal and sub-tidal structures of the sea level and currents of the sub-regions. The basis for separate models is historical, but it is also explained by the fact that the SEACOOS sub-regions (CGB, EFS, and WFS) are characterized by significantly different geometries, tidal regimes, and boundary current forcing that require focused attention (*Boicourt et al., 1998*). The entire SEACOOS region is linked by the advection of the Gulf of Mexico Loop Current (LC), Florida Current (FC), and Gulf Stream (GS) complex. The SAB from North Carolina to the Northeast Florida Shelf is narrow at Cape Hatteras, broad in the middle, and narrow at Cape Canaveral with varying impacts by the GS; the Southeast Florida Shelf is very narrow and always abutted by the FC; and the WFS is generally very wide

and only occasionally impacted by the LC. Similar differences exist in the freshwater discharges to these three sub-regions. All are affected, however, by the synoptic scale weather systems that regularly transit the SEACOOS domain. The modeling efforts by UNC, UM and USF were initiated for specific sub-regional purposes and are evolutionary. Here, an initial attempt at merging the output from these models to describe the response to a pair of strong weather events in March 2001 is provided. As a starting point, all three sub-regional models omit forcing from deep-ocean boundary currents (LC, FC, and GS) and aim at addressing the following set of questions:

1. Can three separate sub-regional ocean models provide a coherent description of the coastal ocean circulation in the SEACOOS domain under relatively coherent and strong forcing from synoptic scale weather events?
2. To what degree do the sub-regional models reproduce *in-situ* observations?
3. What might be done to improve the models' fidelity?

The paper is organized as follows. Section 2 introduces the three sub-regional modeling systems. Using *in-situ* data, Section 3 describes atmospheric and oceanic conditions during two March 2001 storm passages, one in early March and the other in late March. Section 4 presents the model results and the model/data comparisons for each sub-region, and Section 5 offers a discussion, followed by a summary in Section 6.

## **2. SEACOOS sub-regional coastal ocean models**

The coastal ocean circulation models used in SEACOOS sub-regions are the Dartmouth College Ocean Model: QUODDY for CGB (at UNC) and the Princeton Ocean Model: POM for EFS (at UM) and WFS (at USF). QUODDY is a finite-element circulation model (*Lynch et al.*, 1996). The model is three-dimensional, hydrostatic, Boussinesq, fully nonlinear, and has a free surface. It integrates momentum, temperature and salinity, and two turbulence variables. Both barotropic and baroclinic motions are resolved on tidal time scales. QUODDY uses unstructured meshes of triangles to facilitate variable horizontal resolution. A general terrain-following vertical coordinate system is also used, with non-uniform vertical discretization, which allows tidal-time tracking of the free surface and resolution of surface and bottom boundary layers.

POM (*Blumberg and Mellor, 1987*) has similar attributes, i.e., terrain-following, fully nonlinear, hydrostatic, Boussinesq, free surface, and vertical and horizontal turbulence parameterization. However, POM employs a finite difference scheme in an orthogonal curvilinear coordinate system and uses a split time-stepping technique to separate the external mode (vertically integrated 2-D transport and sea surface height) from the internal mode (3-D momentum, temperature, salinity, and turbulence structures). In all three sub-regional model implementations, vertical mixing is represented by a level 2.5 turbulence closure scheme (*Mellor and Yamada, 1982; Galperin, et al, 1998*), and horizontal mixing is represented by a mesh- and shear-dependent eddy viscosity scheme (*Smagorinsky, 1963*). In each model, the background eddy viscosity (as shown in Table 1) is  $5 \times 10^{-5} \text{ m}^2/\text{s}$ . In summary, the QUODDY implementation covers much of the CGB, while the two POM implementations separately cover the entire EFS and WFS (Fig. 2). Further, the sub-regional model grids are deliberately designed to overlap for comparison and integration purposes.

The three models are used to hindcast the SEACOOS sub-regional ocean responses to the extratropical storm passages of March 2001. For that purpose, the model bottom topography, surface and lateral boundary forcing fields, initial conditions, and model parameters have been made consistent (Table 1). However, some dissimilarities among the three models remain due to differences in numerical schemes, and in implementations of lateral and surface boundary conditions (Table 2).

Although the individual models use different global tidal databases to prescribe the tides along their respective open boundaries (OBs), comparisons among the three global tidal models indicate that tidal amplitudes and phases of the tidal constituents included in the three SEACOOS sub-regional models are essentially the same (*Blanton et al., 2004*).

### **3. March 2001 storms: what is known from the *in-situ* data?**

Two intense storms passed through the SEACOOS domain around March 5 to 9 and March 20 to 24, 2001. The surface wind and pressure fields of these synoptic storms are given by the NECP/NCAR reanalysis called EDAS (Fig. 3). The first storm is a typical Nor'easter. Its center passes through between 35N and 40N to the north of the SEACOOS domain. Strong pressure gradients drive strong southeastward winds of speeds up to  $25 \text{ m s}^{-1}$  during March 5-8. The storm lasts about 2 days at most locations, and then weakens when the low-pressure system

moves northeastward. This is a large weather system and the resultant surface atmospheric fields over the SEACOOS domain are relatively uniform. The second storm is of a somewhat different nature. It stems from a cyclone originating over the Gulf of Mexico and follows a track well to the south of the first storm. As the storm moves eastward the speed and direction of the wind field change, especially, over Georgia and the Carolinas where the storm center passes through. Maximum wind speed reaches up to  $20 \text{ m s}^{-1}$ . This storm is smaller and has a more spatially heterogeneous wind field over the SEACOOS domain than the first storm.

Winds force coastal currents both directly and through the upwelling (downwelling) variations in sea level by the Ekman divergence (convergence) at the coastal boundary. The coastal ocean response to wind forcing is determined by strength and duration of the wind stress, density stratification, bottom topography, and coastline configuration. Along the relatively straight WFS coastline, southeastward winds during the first and second storms are upwelling-favorable. In contrast, the same wind fields on the EFS are downwelling-favorable. Moving north to the CGB, where the coastline bends toward the northeast, the same winds drive water offshore to again become upwelling favorable. Hence, due to differences in coastlines alone, the SEACOOS regional scale ocean responses to storms are expected to be heterogeneous even with a relatively uniform and persistent wind field.

Time series of both atmospheric and oceanic *in-situ* observations offer a detailed view of the storm and ocean response evolutions. [Here, the interest is in subtidal variations so all time-series are low-pass filtered (with a cutoff of 40 hr).] The wind, air temperature, water temperature, and surface pressure observed by the NDBC [National Data Buoy Center] buoy 42036 on the WFS are examined (Fig. 4). At this location, during the first storm (March 5 to 8), sea surface pressure rises about 10 mb, and the surface air temperature drops about  $8^{\circ}\text{C}$ . In response to the atmospheric forcing, the water temperature drops about  $2^{\circ}\text{C}$ , probably due to both the surface cooling and the coastal upwelling induced by strong southeastward winds (*He and Weisberg, 2002*). After the cyclone develops and passes by the site during the second half of the month, surface air and water temperatures increase by 5 and  $1^{\circ}\text{C}$ , respectively, between March 21 and 24. The surface air pressure also increases as the cooler, high-pressure system replaces the previous, warmer low-pressure system. Observations from other NDBC buoys across the SEACOOS region, when viewed together (Fig. 5), indicate the temporal and spatial variations of the wind field. Based on the wind time-series measured by the buoys and a C-

MAN station located at the central WFS (42036), the Dry Tortugas (DRYFL), the Straits of Florida (41009), and the SAB (41004), and in agreement with the NCEP analyzed winds, the first storm is indeed a larger cyclone, with the quite spatially uniform wind fields across the SEACOOS domain. The second storm is a smaller cyclone, with wind fields having greater temporal and spatial variability. The NCEP analyzed winds are compared with observed winds at the same selected locations. Note that while the NCEP analyzed winds are sampled at 10 m above the sea surface, the observed winds from different stations are observed at different anemometer heights (varying from 2 to 5 m) above the sea surface. To remove that inconsistency, the observed winds are rescaled from their respective anemometer heights to 10-m with the scheme of *Large and Pond* (1981). A complex correlation analysis (*Kundu, 1976*) is then used to quantify these wind comparisons. The complex coefficient has both an amplitude and a phase, the amplitude being the correlation coefficient *per se* and the phase being the angle (in degrees measured counter-clockwise) between the analyzed and observed winds. The regression coefficient is also calculated to account for the NCEP model's ability to reproduce the speed of the observed winds. It is found that the NCEP model underestimates *in-situ* winds by up to 30 percent at some locations (Fig. 5). Although all correlation coefficients are above 0.8, some temporal variability is clearly missing in NCEP wind fields.

Coastal ocean responses to these extratropical storms are manifested in coastal sea level time series (Fig. 6) from the tide gauges distributed along the SEACOOS coast from the CGB to the WFS (Fig. 1). During the first storm, large-scale southeastward winds cause coastal sea levels to drop along both the WFS coast and the CGB coast. During the second storm, the winds on the WFS are largely upwelling-favorable, while the winds on the CGB change direction from onshore (downwelling-favorable) to offshore (upwelling-favorable), causing sea level to first rise and then subside during this event. Sea level variations on the EFS are much less pronounced than on the WFS and the CGB. This difference in coastal sea level variability may be related to the much narrower shelf, and the closer proximity of the FC, along the EFS.

#### **4. March 2001 storms: what is known from the ocean model simulations?**

The model experiments are conducted under three scenarios (Table 3), each with increasing complexity: exclusion or inclusion of tides and the exclusion or inclusion of density stratification. Deep-ocean forcing by boundary currents is omitted in all experiments in order to

focus on the SEACOOS coastal ocean subtidal response to the storms. The NCEP analyzed winds are used for all scenarios in each of the individual sub-regional model runs; the resultant solutions are then compared with observations to assess model performance, discrepancies relative to the field observations, and pathways toward model improvements.

Cases I and II are barotropic experiments with uniform density, and thus, they are intended to identify the importance of elevated friction (due to tidal currents) in the barotropic shelf responses to synoptic weather forcing. Of the three sub-regions, the largest tides are in the CGB. Stratification plays an important role in the coastal ocean circulation by suppressing mixing and by reducing bottom friction through baroclinic compensation of the surface pressure field and, hence, decreasing the geostrophic interior currents that interact with the bottom topography. In case III, density stratification is introduced by using the sub-region averaged density profiles for the initial density field. A more realistic 3-dimensional density field initialization is not attempted here because SEACOOS-wide, synoptic hydrographic data are not available for March 2001. Case III is, thus, admittedly, a simplistic, process-oriented experiment that will require future improvements to accommodate the fully three-dimensional aspects of the stratification, especially in EFS where the stratification is largely determined by the baroclinic FC. Since the onset of the spring transition occurs in March, the stratification introduced in Case III is relatively weak compared to the stratification in late spring and summer.

For hindcast verifications, modeled coastal sea levels are compared with observed values at NOS coastal tide gauges, and modeled currents are compared with observed values at mooring locations throughout the SEACOOS domain (Fig. 1). The level of agreement between the hindcast and observations is quantified by the correlation coefficients and the *rms* misfit values for the sea levels, and by the complex correlation coefficients and regression coefficients for the currents.

## **4.1. Sea Level Comparisons**

### **4.1-A. CGB**

Comparisons made at Fort Pulaski, St. Augustine and Fernandina Beach are considered in CGB (Fig. 7). In general, the CGB model captures the sea level changes induced by the two extratropical storm passages. The correlation coefficients are greater than 0.84, and *rms* misfits are less than 0.12 m at all stations. Hindcast sea levels in Case II are essentially the same as

hindcast sea levels in Case I, suggesting that while tidal friction is important on the tidal time scale, it is not critical to the barotropic responses at sub-tidal time scales. Adding stratification in Case III improves the model performance, especially for the second storm passage, which is likely due to reduced bottom friction.

#### 4.1-B. EFS

The EFS model domain overlaps with part of the CGB and part of the WFS, so the comparisons are made at both Gulf coast (Naples, Key West) and Atlantic coast (Virginia Key, Trident Pier, and Fernandina Beach) stations (Fig. 8). Comparisons between the hindcast and observed sea levels indicate that the model that includes tides and local atmospheric forcing only is insufficient to represent the sub-tidal variability. Some changes are seen in the correlation coefficients and *rms* misfits between Cases I and II, which range from 0.4 to 0.9 and 0.06 to 0.15 m, respectively. But essentially, as in the CGB model, the similarity between the two cases suggests tidal friction does not much affect the sub-tidal time scale barotropic responses. In Cases I and II, perturbation amplitudes and correlations are relatively high at stations (Fernandina Beach and Naples) adjoining a wide shelf, while they are relatively low at stations (Virginia Key and Key West) adjoining a narrow shelf. Moreover, adding density stratification in Case III does not improve the model skill. (In fact, it generally appears to worsen the solution.)

#### 4.1-C. WFS

Hindcast and observed sea level comparisons are provided at the Apalachicola, Cedar Key, St. Petersburg, and Naples coastal stations in WFS (Fig. 9). Comparisons indicate considerable model skill in capturing the sub-tidal variability, as demonstrated by correlation coefficients of  $\sim 0.9$  and *rms* misfits of  $\sim 0.06$  m at all stations. Moreover, Cases I and II reveal the same finding that tidal friction is relatively unimportant for sub-tidal barotropic sea level variations. Adding stratification basically produces the same model solutions as the barotropic runs using uniform density as specified in Cases I and II, although this finding must be tempered by the fact that the March 2001 stratification is weak. Other WFS simulations with strong stratification have demonstrated that the response to synoptic weather systems is stratification-sensitive for reasons related to the frictional bottom boundary layer (e.g., *Weisberg et al.*, 2001).

## 4.2. Current Comparisons

Some limited *in-situ* current observations (Fig. 1) are also available during March 2001 for the SEACOOS domain. These *in-situ* velocity measurements allow comparisons between hindcast and observed currents, and provide additional skill evaluations of CGB, EFS and WFS models. The same complex correlation analysis as applied earlier to the surface wind comparisons is used to quantify these current comparisons. The regression coefficient is also calculated to account for the model's ability to hindcast the speed of the observed currents. Time series of hindcast currents are extracted from the Case III runs for the CGB and the WFS, and from the Case II run for the EFS. This procedural variation is made because, as in the EFS coastal sea level comparison presented above, adding simplified density stratification in Case III degrades the EFS model skill in current hindcasts; hence, hindcast currents from Case II are used for the EFS to provide model current skill assessment under the constant density scenario.

For the CGB, the depth-averaged current comparison at the 25 m isobath (Fig. 10) indicates that the model reproduces the patterns of current variability with a correlation coefficient of 0.8, and the orientation misfit of less than  $5^\circ$ . Additional discrepancies include a strong southeastward current missing in the model solution during the first storm and that the hindcast current underestimates the observed velocity fluctuations by 50 % (as shown by 1 minus the regression coefficient). Case II produces currents similar to those of Case III; however, the hindcast in Case II (not shown) underestimates the observed velocity fluctuations a little further (by 55%). This is likely because the bottom friction is elevated in the absence of density stratification. For the EFS, the comparison (Fig. 12) is made at mid-depth at the 10 m isobath off the Florida Keys. Except for missing two strong southwestward flows in the middle of March, the hindcast generally reproduces the patterns of observed current variability with a correlation coefficient of 0.7 and orientation misfit of  $-8^\circ$ , but the speeds of the hindcast current are much weaker, only 40 % of observed velocity fluctuations. For the WFS, current comparisons are made between the hindcast and observed velocities at mid-depth at the 10m (Fig. 12), 20m, and 30m (not shown) isobaths. The WFS model captures the sense of the velocity rotation correctly at all locations. The correlation coefficients range between 0.9 and 0.7 and orientations agree to within  $\pm 3^\circ$ . Model performance degrades as comparison sites are located further away from the coast. Based on the regression coefficients at all three across-shelf stations, the model underestimates the observed currents by between 40 and 60 %, comparable to the CGB and the

EFS model results. Consistent with sea level comparisons presented above, Case II (not shown) produces essentially the same current hindcasts as Case III., again suggesting that the effect of the March 2001 stratification is weak and that the WFS circulation response is largely barotropic.

## 5. Discussion

The systematic underestimation of the observed current speeds by all three sub-regional models is probably a result of the underestimation of the observed wind speeds by NCEP analysis as demonstrated (Fig 5). Given that wind stress is a nonlinear function of wind speed, these discrepancies in wind speeds can likely, in a nonlinear way, lead to amplified errors in wind stresses, which could help explain why the hindcast current speeds are too weak. When forced by these surface winds, inaccuracies in the surface forcing field propagate into the ocean models, causing inaccurate ocean circulation hindcasts that can be improved on by improving the surface forcing (*He et al.*, 2004).

Sea level time series along coastal ocean domains often indicate the along shelf propagation of continental shelf or coastally trapped waves (e.g., *Gill*, 1981). Visual examination of limited sea level time series of only a month-duration (Fig. 6) however yields no clear indication of such freely propagating waves in the SEACOOS region. Their absence may be a consequence of forced wave dominance, high dissipation levels over broad, shallow shelves (*Pietrafesa and Janowitz*, 1980), complex interference caused by scattering, and damping patterns associated with the heterogeneous responses due to varying coastline orientations, shelf widths, and boundary currents. For instance, the strong shear on the shelf in the mean alongshore currents can significantly enhance coastally trapped wave damping when the boundary current has cyclonic relative vorticity (*Brink*, 1990; *Schumann and Brink*, 1990) as occurs in the SEACOOS domain. Alternatively, the coastally trapped waves may not be manifested in coastal sea level, which would necessitate examining current or other observations on the outer shelf, for example, to detect them.

Based on the comparisons between *in-situ* observations and hindcasts, the CGB and WFS models have considerable skill at capturing sub-tidal time scale variations in both coastal sea level and currents during these storm events. The EFS model is relatively less skillful, especially in Case III. This result is not a generic weakness of the model itself but, rather, it reflects the sub-regional complexity. One reason for the better skill of the CGB and WFS models is that their

offshore lateral boundary are located in the deep ocean away from the shelf, which helps minimize the adverse effect of inaccurate (sub-tidal) deep ocean boundary values and allows the wind-driven circulation to more fully develop. A second reason is that broad shelf width provides for small Burger number such that the barotropic approximation is theoretically justifiable on the WFS (*Clarke and Brink, 1985*), and possibly on the CGB as well, as further attested to by Case III. The EFS model's reduced skill may arise for several reasons. First, it may be necessary to refine the coastline and increase the resolution in a "coastal strip" over the shelf. Second, realistic 3-dimensional baroclinicity from the adjacent FC is absent in these EFS model simulations. Given the importance of the adjacent FC, local atmospheric forcing, together with the highly simplified 1-D density stratification, is not sufficient to account for the observed variability. Third, the Southeast Florida Shelf region (model interior) is very narrow (viz., the shelf is only a few grid points wide) so that the way the lateral boundary conditions (LBC) are treated in the EFS model may have more adverse impact on the model interior solution. Compared to the shelves of the CGB and WFS, the Southeast Florida Shelf is narrow and presumably less dissipative. In addition, within the Straits of Florida, the offshore boundary of the EFS sub-regional model is largely a solid barrier comprised of Cuba and the Bahamas, except for its channels open to the Atlantic Ocean. More accurate LBC specifications are necessary for this sub-regional model (likewise, CGB and WFS models) to better account for sub-tidal variability, dictating a dynamically sound nesting approach that couples sub-regional models with a larger domain, open ocean model.

While baroclinicity has already been utilized by each sub-regional model to produce more realistic simulations and validate against *in situ* observations (e.g., *Weisberg et al. 2001*; *Weisberg and He, 2003*; *He et al., 2004*; *Fiechter and Mooers, 2003*; *Mooers and Fiechter, 2005*), the quasi-operational runs of each model as part of the integrated products of SEACOOS (<http://seacoos.org>) are currently barotropic (for sub-tidal scale, this is equivalent to Case I shown herein). It is therefore of interest to assess the temporal and spatial variability of coastal ocean responses produced by the three sub-regional models and their ability to achieve coherent descriptions and accurate predictions of the state and evolution of the SEACOOS coastal ocean environment. To do that, sub-tidal hindcast fields (Case I) are sampled on the mid-days of March 4 to 7 for the first storm passage, and on the mid-days of March 20 to 23 for the second storm passage. During the first storm, the SAB responds to the strong southeastward wind with a

major coastal upwelling (Fig. 13, upper four panels). The maximum sea level set-down (ca. 0.4 m) occurs along the Georgia coast on March 5 to 6. During the second storm (Fig. 13, lower four panels), the SAB changes from a downwelling response to an upwelling response as the smaller scale cyclonic storm passes by and changes the wind direction from northwestward to southeastward. Similar scenarios for the spatial and temporal evolution of sea level and surface currents occur on the EFS (Fig. 14). The WFS responds to both storms (Fig. 15) with strong coastal upwelling. The maximum currents and sea level set-downs occur on March 6 during the first storm passage, and on March 21 during the second storm passage.

To quantify the model solutions in the overlapping regions of three sub-regional models, means and standard deviations of absolute hindcast (Case I) sea level mismatches are calculated separately over the period of each of the two storm passages (Fig. 16). During each period, maximum mean misfits of the order of 0.1 m are found in the coastal waters offshore of Florida and Georgia border. Some mismatches of smaller magnitude are also seen in the Florida Keys area. Driven by local atmospheric forcing, the three sub-regional models produce quantitatively similar coastal circulation in the overlapping regions; although some discontinuities in the quantitative details between the adjacent (CGB-EFS, and EFS-WFS) model solutions presently exist.

## 6. Summary

Starting with three existing sub-regional coastal ocean models, an effort has been presented to link them to form the initial basis for the modeling component of SEACOOS. By coordinating *in-situ* observations with models, SEACOOS endeavors to provide an integrated description of the synoptic circulation of the southeast U.S. coastal ocean. Here, the sub-tidal coastal ocean sea level and current responses to synoptic weather forcing are of particular interest because such responses are important to storm surges and material property transports in the coastal ocean environment. As a preliminary assessment of the three sub-regional models, the hindcasts of the local wind-driven circulation are commenced by considering responses to extratropical storm passages in March 2001. Open ocean boundary currents are neglected. Tidal solutions are prescribed along the open boundaries of all three sub-regional models from global tidal models. Each of three models considered three scenarios in order to discern the contributions of tidal friction and density stratification. For all three sub-regions, adding tidal

friction does not significantly affect the sub-tidal model solutions, suggesting that added tidal friction is relatively unimportant in the SEACOOS coastal ocean region. Adding an idealized stratification (a density profile) improves the model solutions on the CGB, but worsens the solutions on the EFS, and does not much change the solutions on the WFS (for these particular events). In reality, the stratification on the EFS is 3-dimensional, and primarily a consequence of the adjacent baroclinic FC, which is not included herein; and on the WFS impacts by the LC at the shelf slope can affect the stratification and the shelf circulation very importantly under certain scenarios (*Weisberg and He, 2003*).

Comparisons between *in-situ* observations and model hindcasts are made for each of the sub-regional models. The CGB and WFS models demonstrate considerable skill at capturing sub-tidal time scale variations in both sea level and currents. The EFS model is less skillful. For all three sub-regional models, a more dynamically consistent and physically sound approach to better specify sub-tidal LBCs would be to nest the sub-regional models in basin-scale or global models. In fact, efforts have now been made to embed each of three sub-regional models in data assimilative, basin-scale or global OGCMs.

High quality surface forcing specification is also a critical factor in coastal ocean modeling (*He et al., 2004*), some inaccuracies of 3-hr, 32-km NCEP analyzed wind fields utilized herein are clearly demonstrated when gauged against *in-situ* buoy and coastal station wind observations and pose the necessity of using newly available, higher resolution atmospheric forcing fields (e.g., the NCEP/NCAR ETA 12 km product) of presumably better accuracy.

In summary, improving the overall SEACOOS modeling effort requires consistent specification of lateral boundary conditions at sub-tidal time scales. Additionally, specification of 3-dimensional baroclinicity and, thus, inclusion of ocean boundary currents are also high priorities. As global scale operational models emerge (e.g., Global-NCOM, *Barron et al., 2003*), and as alternative basin scale modeling efforts (e.g., HYCOM, *Chassignet et al., 2003*) further mature, they provide promise for SEACOOS sub-regional modeling efforts to achieve these goals through model nesting. SEACOOS is also building an extensive regional observing system (*Seim et al., 2003*), and as data streams from multiple sensors and platforms become available, model skill assessment can be expanded and application of data assimilation techniques may further assist in model estimation improvements. Regardless of open boundary forcing and interior data assimilation, however, a primary limitation to coastal ocean modeling resides in the

external forcing fields themselves. Only through the coordinated efforts of *in-situ* monitoring and modeling will the necessary improvements be achieved, both for the coastal ocean and the coastal atmosphere. As an emergent coastal ocean observing system, this is a SEACOOS goal.

### **Acknowledgements**

This manuscript is a contribution to the SEACOOS Program sponsored by ONR. Mr. Jerome Fiechter is thanked for providing the curvilinear grid used by the EFS model. Dr. Tom Lee is thanked for making available observed current time series for the Florida Keys.

## References

- Bane, J. M., 1989: Results from the genesis of Atlantic Lows Experiment Physical Oceanographic Studies: Introduction, *Journal of Geophysical Research*, 94, 8, 10685.
- Bane, J. M, K. E. Osgood, 1989: Wintertime Air-sea interaction processes across the Gulf Stream, *Journal of Geophysical Research*, 94, 8, 10,755-10,772.
- Barron, C.N., R. C. Rhodes, L. F. Smedstad, P. J. Martin, and A. B. Kara, 2003: Global Ocean Nowcasts and Forecasts with the Navy coastal ocean model (NCOM), 2003 NRL Review, 175-178.
- Blanton, J. O., J. A. Amft, D. K. Lee, and A. Riordan, 1989: Wind stress and heat fluxes observed during winter and spring 1986, *Journal of Geophysical Research*, 94, 8, 10,686-10,698.
- Blanton, B. O., A. Aretxabaleta, F. E. Werner, and H. E. Seim, 2003: Monthly climatology of the continental shelf waters of the South Atlantic Bight, *Journal of Geophysical Research*, 108(C8), 3264, doi:10.1029/2002JC001609.
- Blanton, B., I. Bang, R. He, 2004: Implementation of the SEACOOS Nowcast/Forecast Model System Version 1.0: Barotropic Models and Skill. SEACOOS MPCC report (unpublished manuscript).
- Blumberg, A. F. and G. L. Mellor, 1987: A description of a three-dimensional coastal ocean circulation model. In: Three-Dimensional Coastal Ocean Models, edited by N. Heaps, 208 pp., American Geophysical Union.
- Boicourt, W.C., W.J. Wiseman Jr., A. Valle-Levinson and L.P. Atkinson, 1998: Chapter 6. Continental Shelf of the Southeastern United States and the Gulf of Mexico: In the Shadow of the Western Boundary Current. In *The Sea*, 11, 135-181. K.H. Brink and A.R. Robinson eds., Wiley, N.Y.
- Brink, K. H., 1990: On the damping of free coastal-trapped waves, *Journal of Physical Oceanography*, 20, 1219-1225.
- Brooks, D.A. and C. N. K. Mooers, 1977a: Wind-forced continental shelf waves in the Florida Current, *Journal of Geophysical Research*, 82, 18, 2569-2576.
- Brooks, D. A. and C. N. K. Mooers, 1977b: Free, stable continental shelf waves in a sheared, barotropic boundary current, *Journal of Physical Oceanography*, 7, 3, 380-388.
- Clarke, A. J. and K. H. Brink, 1985: The response of stratified, frictional flow of shelf and slope waters to fluctuating large-scale, low frequency wind forcing. *Journal Physical Oceanography*, 15, 439-453.

- Chassignet, E.P., L.T. Smith, G.R. Halliwell, and R. Bleck, 2003: North Atlantic simulation with the HYbrid Coordinate Ocean Model (HYCOM): Impact of the vertical coordinate choice, reference density, and thermobaricity. *Journal of Physical Oceanography*, 33, 2504-2526.
- Fiechter, J. and C. N. K. Mooers, 2003: Simulation of frontal eddies on the East Florida Shelf, *Geophysical Research Letter*, 30 (22), 2151, doi: 10.1029/2003GL018307.
- Galperin, B., L. H. Kantha, S. Hassid and A. Rosati, 1988: A quasi-equilibrium turbulent energy model for geophysical flows, *Journal of Atmospheric Science*, 45, 55-62.
- Gill A. E., 1982: *Atmosphere-Ocean Dynamics*, pp 408-415, Academic Press, San Diego
- Gu, G. and C. Zhang, 2002: Cloud components of the Intertropical Convergence Zone. *Journal of Geophysical Research*, 107(D21), 4565, doi:10.1029/2002JD002089, 2002.
- He, R. and R. H. Weisberg (2002): West Florida shelf circulation and temperature budget for the 1999 spring transition. *Continental Shelf Research*, 22, 719-748
- He, R., Y. Liu and R. H. Weisberg (2004): Coastal ocean wind fields gauged against the performance of an ocean circulation model. *Geophysical Research Letters*, 31, 14, 14303, doi:10.1029/2003GL019261.
- Hsu, S. A. 1995: A proper wind-stress drag coefficient formulation for computer modeling of seas and coastal regions. *Computer Modeling of Seas and Coastal Regions II*, edited by C. A. Brebbia, L. Traversoni, and L.C. Wrobel, Computational Mechanics Inc. Boston.
- Kundu, P. K, 1976: An analysis of inertial oscillations observed near the Oregon coast. *Journal of Physical Oceanography*, 6, 879-893.
- Large, W. G. and S. Pond, 1981: Open Ocean Momentum Flux Measurements in Moderate to Strong Winds. *Journal of Physical Oceanography*, 11, 3, pp. 324-336.
- Lee, T. N., E. Williams, J. Wang, R. Evans, and L. Atkinson, 1989: Response of South Carolina continental shelf waters to wind and Gulf Stream forcing during winter of 1986, *Journal of Geophysical Research*, 94, 8, 10,715-10,754.
- Lynch, D. R., J. T. C. Ip, C. E. Naimie and F. E. Werner, 1996: Comprehensive coastal circulation model with application to the Gulf of Maine. *Continental Shelf Research*, 16, 875-906.
- Mellor, G. L. and T. Yamada, 1982: Development of a turbulence closure model for geophysical fluid problems. *Reviews of Geophysics and Space Physics*, 20, 851-875.
- Mooers, C.N.K. and J. Fiechter, 2005: Numerical simulation of mesoscale variability in the Straits of Florida. *Ocean Dynamics*, (under revision).

- Peng, G. , C.N. K. Mooers, and H.C. Graber, 1999: Coastal winds in South Florida. *Journal of Applied Meteorology*, 38, 1740 -1757.
- Pietrafesa, L.J, and G. S. Janowitz, 1980: Lack of evidence of southerly propagating continental shelf waves in Onslow Bay, N.C., *Geophysical Research Letters*, 7, 113-116.
- Seim, H.; B. Bacon; C. Barans; M. Fletcher; K. Gates; R. Jahnke; E. Kearns; R. Lea; M. Luther; C. Mooers; J. Nelson; D. Porter; L. Shay; M. Spranger; J. Thigpen; R. Weisberg; F. Werner, 2003: SEACOOS - A Model for a Multi-State, Multi-Institutional Regional Observation System, *Marine Technology Society Journal*, 37, 3, 92-101.
- Schumann, E.H., and K. H. Brink, 1990: Coastal-trapped wave off the coast of South Africa: generation, propagation and current structures, *Journal of Physical Oceanography*, 20, 1206-1218.
- Smagorinsky, J., 1963: General circulation experiments with the primitive equations I. The basic experiment. *Monthly Weather Review*, 91, 99-164.
- Weisberg, R.H. and L.J. Pietrafesa, 1983: Kinematics and correlation of the surface wind field in the South Atlantic Bight. *Journal of Geophysical Research*, 88, 4593-4610.
- Weisberg, R.H., Z. Li, and F. Muller-Karger, 2001: West Florida Shelf response to local wind forcing: April 1998. *Journal of Geophysical Research*, 106, 31,239-31,262.
- Weisberg, R.H. and R. He, 2003: Local and deep-ocean forcing contributions to anomalous water properties on the West Florida Shelf. *Journal of Geophysical Research*, 108, C6, 3184, doi:10.1029/2002JC001407.

**Table 1. Model Attributes**

Attributes	UNC	UM	USF
Horizontal resolution	0.1-50 km	2-10 km	2-6 km
Time Step (seconds)	60	Internal: 40 External: 4	Internal: 360 External: 12
Number of nodes	~10,000	~13,000	~10,000
Vertical sigma levels	21	21	21
Model	Quoddy	POM	POM
Vertical mixing	MY2.5	MY2.5	MY2.5
Horizontal mixing	Smagorinsky C=0.28*	Smagorinsky C=0.2*	Smagorinsky C=0.1*
Background Eddy Viscosity	$5 \times 10^{-5} \text{ m}^2/\text{s}$	$5 \times 10^{-5} \text{ m}^2/\text{s}$	$5 \times 10^{-5} \text{ m}^2/\text{s}$
Wind stress scheme	Hsu (1995)	Hsu (1995)	Hsu (1995)
Inverse horizontal Prandtl number	1	0.2	1
Min. water depth	2 m	2 m	2 m
Max water depth	2000	2000	2000
Bottom drag coefficient	0.0025	Depth-dependent Minimum =0.0025	Depth-dependent minimum =0.0025
Initial T/S profile	Domain averaged Blanton et al (2003) March Climatology	Domain averaged Levitus 98 winter climatology	Domain averaged March 01 shelf hydrography

\*:  $C$  is the free parameter used in the *Smagorinsky* (1963) scheme for quantifying the horizontal mixing.

NOTE: for EFS-POM, external and internal time steps for Case III are given above, while for Cases I and II they are 6 and 180 sec and 4 and 120 sec, respectively.

**Table 2. Surface and Lateral Boundary Conditions**

Attributes	UNC	UM	USF
Global tide model used to extract tidal BC's	FES95D LeProvost	OSU- TPXO.6	CCAR Tierney/Kantha
Number of tidal constituents	$M_2, N_2, S_2, K_2, O_1, K_1, P_1, Q_1$ (8)	$M_2, N_2, S_2, K_2, O_1, K_1, P_1, Q_1$ (8)	$M_2, N_2, S_2, K_2, O_1, K_1, P_1, Q_1$ (8)
Tidal potential	No	Yes	No
Surface fields of momentum and heat flux	32 km, 3-hourly NCEP EDAS surface fields	32 km, 3-hourly NCEP EDAS surface fields	32 km, 3-hourly NCEP EDAS surface fields
Satellite AVHRR SST relaxation	Yes	Yes	Yes
BC's Sea Surface Height	Tides	Tides	Tides
External Velocity 2-D LBC	No-gradient	Radiation	Radiation
Internal 3-D Velocity LBC	No-gradient	Radiation	Radiation

**Table 3. Experimental designs**

<b>Experiment</b>	<b>Tide</b>	<b>Density</b>
Case I	No tides	Barotropic (uniform density)
Case II	With tides	Barotropic (uniform density)
Case III	With tides	Stratified (density profile from Levitus winter climatology [UNC and UM] or shelf observations (USF))

## Figures Captions:

Figure 1. Bottom topography and observation locations in SEACOO domain. Coastal tide gauges are denoted by red dots, NDBC buoys and a C-MAN station by blue triangles, and current meter moorings by circles.

Figure 2. Model grids used to compute circulation on West Florida Shelf (WFS) (green); East Florida Shelf (EFS) (magenta); and Carolina-Georgia Bight (CGB) (cyan)

Figure 3. Snapshots of six-hourly surface wind vectors and surface pressure fields in color (1000 mb is subtracted) fields during two extratropical storm passages (1<sup>st</sup> storm: left four panels, 2<sup>nd</sup> storm: right four panels). Data were obtained from the NCEP/NCAR Reanalysis Project (<http://www.cdc.noaa.gov/cdc/reanalysis/reanalysis.shtml>).

Figure 4. Time series of wind, air temperature, water temperature and surface pressure observed at NDBC buoy 42036 (on the WFS) during March 2001. The shaded intervals indicate the storm passages.

Figure 5. Comparison between observed (by NDBC buoys and a C-MAN station) and analysis (by NCEP EDAS) wind time series. Each pair model/data comparison is quantified by its complex correlation coefficient  $\rho$ , phase angle  $\theta$  (or angular deviation of the model vector from the data vector measured counter-clockwise) in degrees, and regression coefficient  $r$ . The shaded intervals indicate the storm passages.

Figure 6. Time series of observed coastal sea levels during March, 2001, after adjustment for barometric pressure and 40-hr low-pass filtered. The shaded intervals indicate the storm passages.

Figure 7. Comparison between observed and hindcast sea levels in the CGB domain. Cases I, II, III (see Table 3) and observations are in red, blue, black, and gray, respectively. All time series are 40-hr low-pass filtered. The number pair indicates the correlation coefficient and the *rms* difference (m) for each case. The shaded intervals indicate the storm passages.

Figure 8. Comparison between observed and hindcast sea levels in the EFS domain. Cases I, II, III (see Table 3) and observations are in red, blue, black, and gray, respectively. All time series are 40-hr low-pass filtered. The number pair indicates the correlation coefficient and the *rms* difference (m) for each case. The shaded intervals indicate the storm passages.

Figure 9. Comparison between observed and hindcast sea levels in the WFS domain. Cases I, II, III and observations are in red, blue, black, and gray, respectively. All time series are 40-hr low-pass filtered. The number pair indicates the correlation coefficient and the *rms* difference (m) for each case. The shaded intervals indicate the storm passages.

Figure 10. Comparison between observed and hindcast (Case III) depth-averaged currents at SAB Navy tower R2 at 25 m isobath. The model/data comparison is quantified by its complex correlation coefficient  $\rho$ , phase angle  $\theta$  (or angular deviation of the model vector from the data vector measured counter-clockwise) in degrees, and regression coefficient  $r$ .

Figure 11. Comparison between observed and hindcast (Case II) mid-depth currents at EFS Hawk Channel near Looe Key at 10 m isobath. Currents are rotated 90 degrees counter-clockwise, i.e., east is upward. The model/data comparison is quantified by its complex

correlation coefficient  $\rho$ , phase angle  $\theta$  (or angular deviation of the model vector from the data vector measured count-clockwise) in degrees and regression coefficient  $r$ .

Figure 12. Comparison between observed and hindcast (Case III) mid-depth currents at WFS EC5 at 10 m isobath. The model/data comparison is quantified by its complex correlation coefficient  $\rho$ , phase angle  $\theta$  (or angular deviation of the model vector from the data vector measured count-clockwise) in degrees, and regression coefficient  $r$ .

Figure 13. Snapshots of daily hindcast (UNC QUODDY Case I) surface current vectors and sea surface heights in color (m) during the first (upper four panels) and the second (lower four panels) storm passages in CGB.

Figure 14. Snapshots of daily hindcast (UM POM Case I) surface current vectors and sea surface heights in color (m) during the first (upper four panels) and the second (lower four panels) storm passages in EFS.

Figure 15. Snapshots of daily hindcast (USF POM Case I) surface current vectors and sea surface heights in color (m) during the first (upper four panels) and the second (lower four panels) storm passages in WFS.

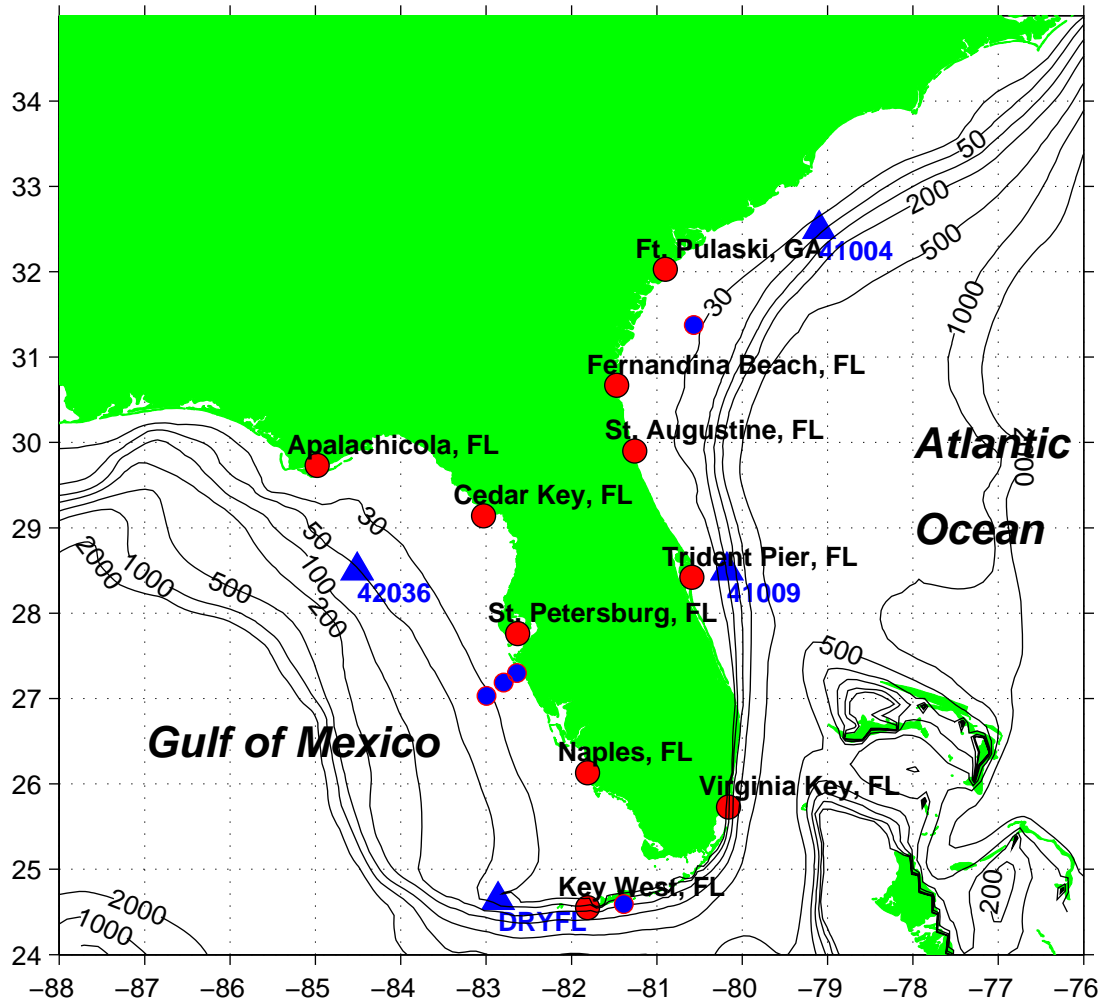


Figure 1. Bottom topography and observation locations in SEACOOS domain. Coastal tide gauges are denoted by red dots, NDBC buoys and a C-MAN station by blue triangles, and current meter moorings by circles.

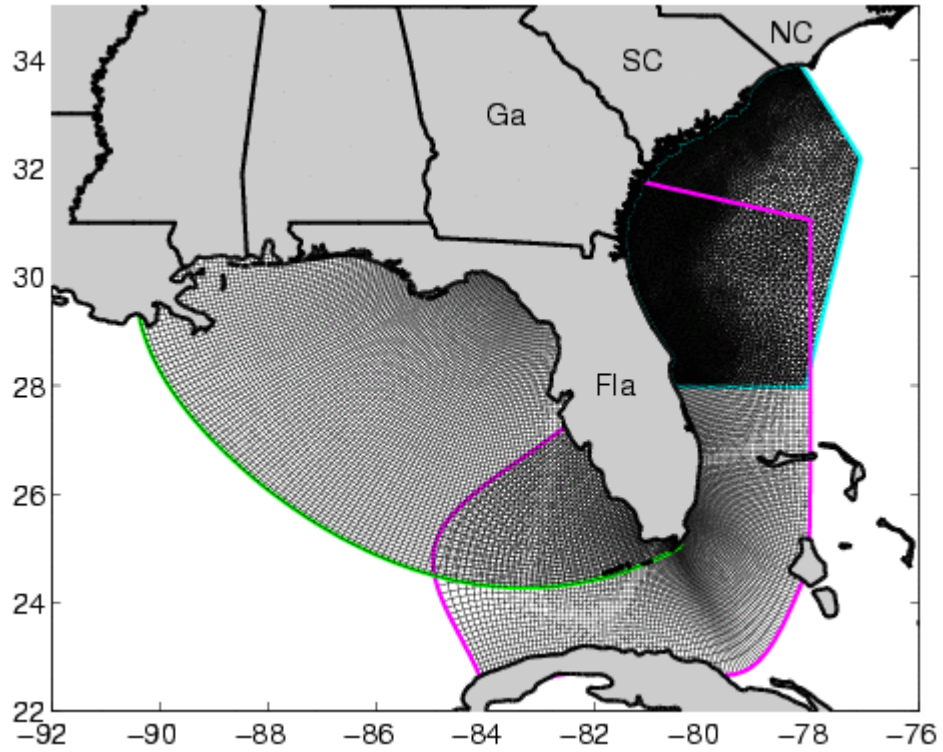


Figure 2. Model grids used to compute circulation on West Florida Shelf (WFS) (green); East Florida Shelf (EFS) (magenta); and Carolina-Georgia Bight (CGB) (cyan)

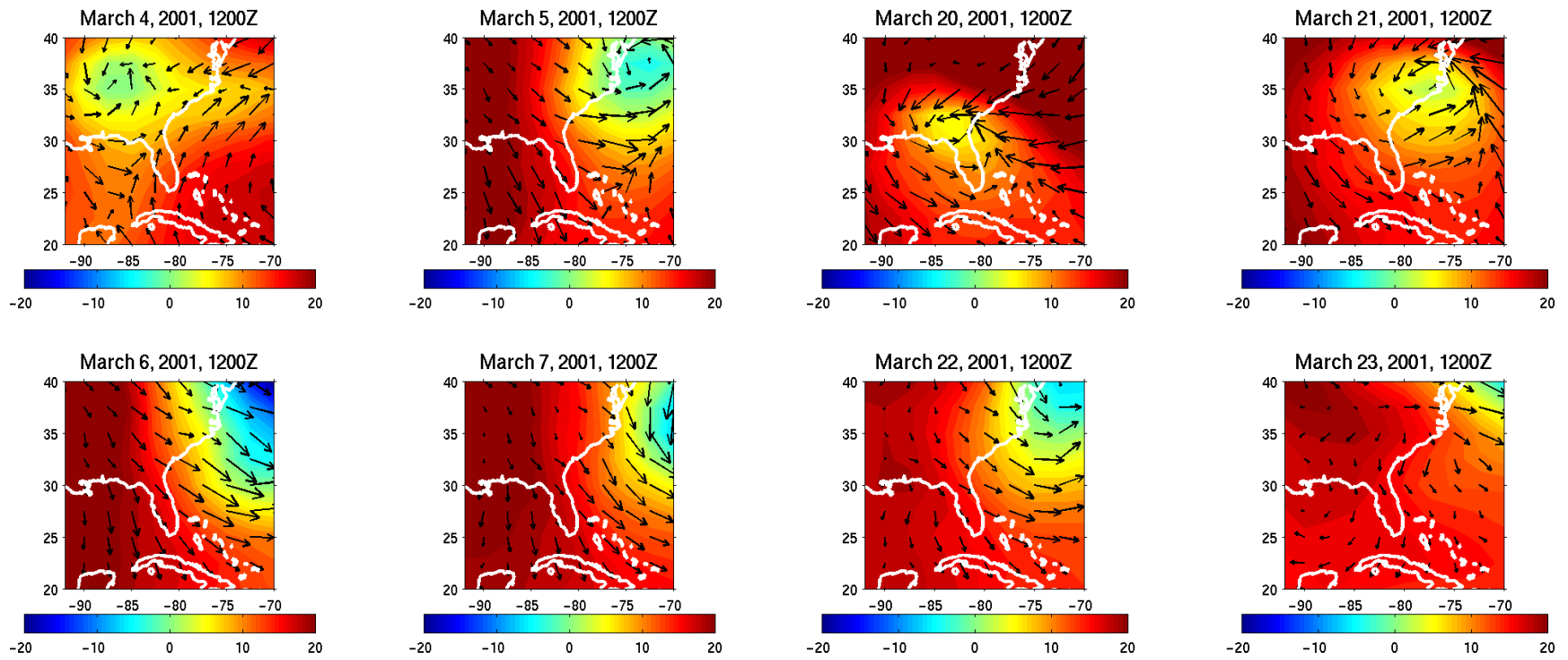
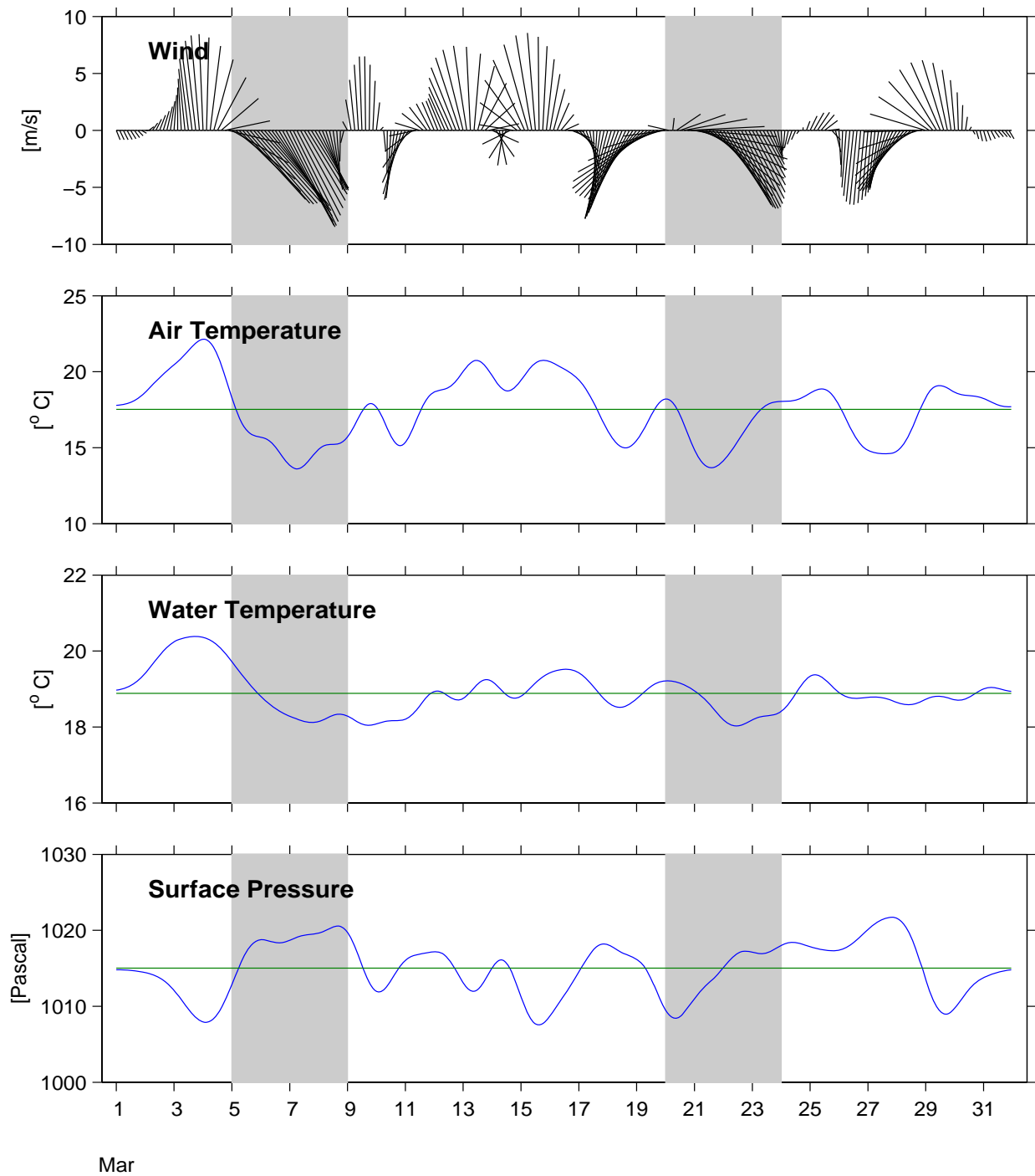


Figure 3. Snapshots of six-hourly surface wind vectors and surface pressure fields in color (1000 mb is subtracted) fields during two extratropical storm passages (1<sup>st</sup> storm: left four panels, 2<sup>nd</sup> storm: right four panels). Data were obtained from the NCEP/NCAR Reanalysis Project (<http://www.cdc.noaa.gov/cdc/reanalysis/reanalysis.shtml>).



2001

Figure 4. Time series of wind, air temperature, water temperature and surface pressure observed at NDBC buoy 42036 (on the WFS) during March 2001. The shaded intervals indicate the storm passages.

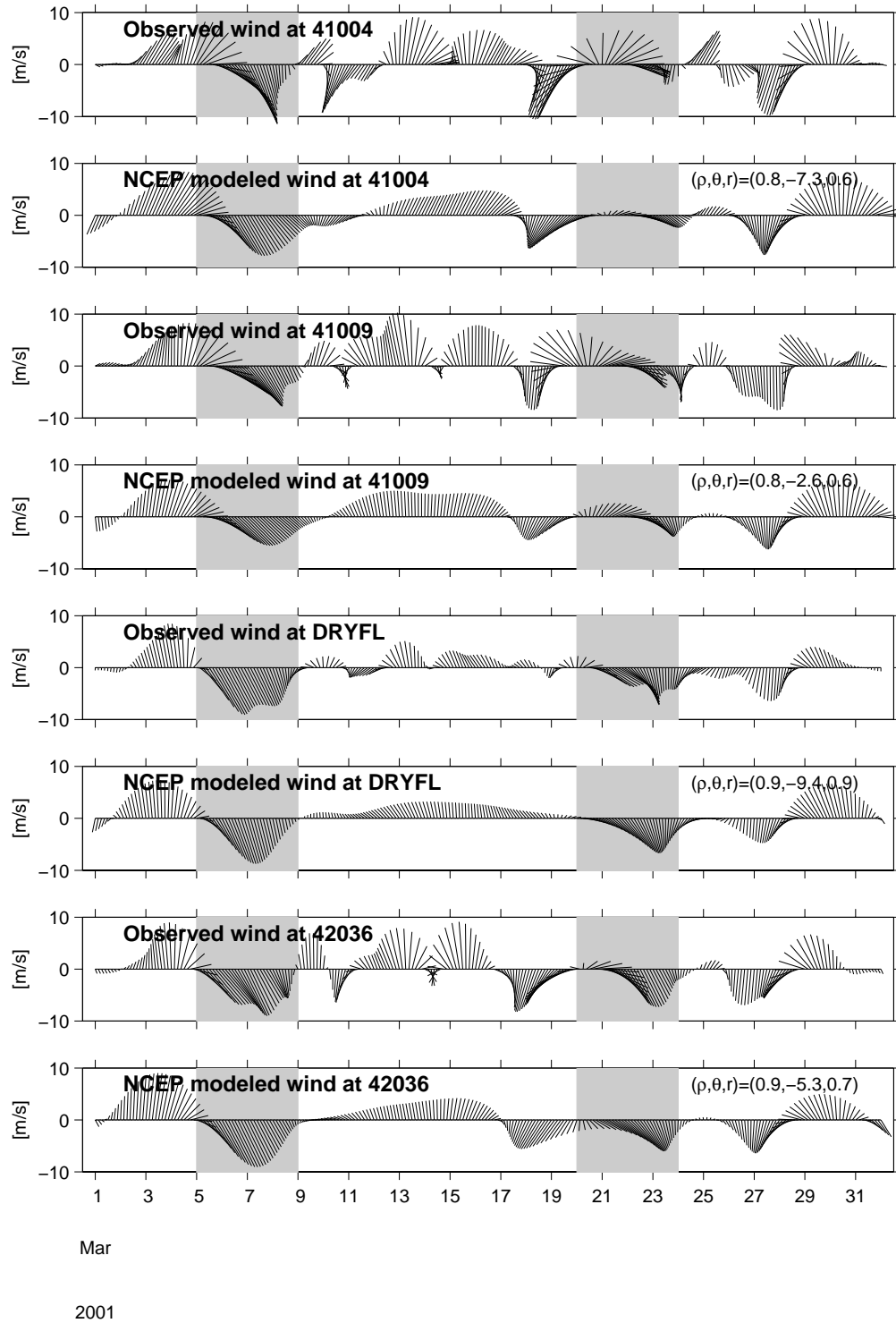


Figure 5. Comparison between observed (by NDBC buoys and a C-MAN station) and analysis (by NCEP EDAS) wind time series. Each pair model/data comparison is quantified by its complex correlation coefficient  $\rho$ , phase angle  $\theta$  (or angular deviation of the model vector from the data vector measured counter-clockwise) in degrees, and regression coefficient  $r$ . The shaded intervals indicate the storm passages.

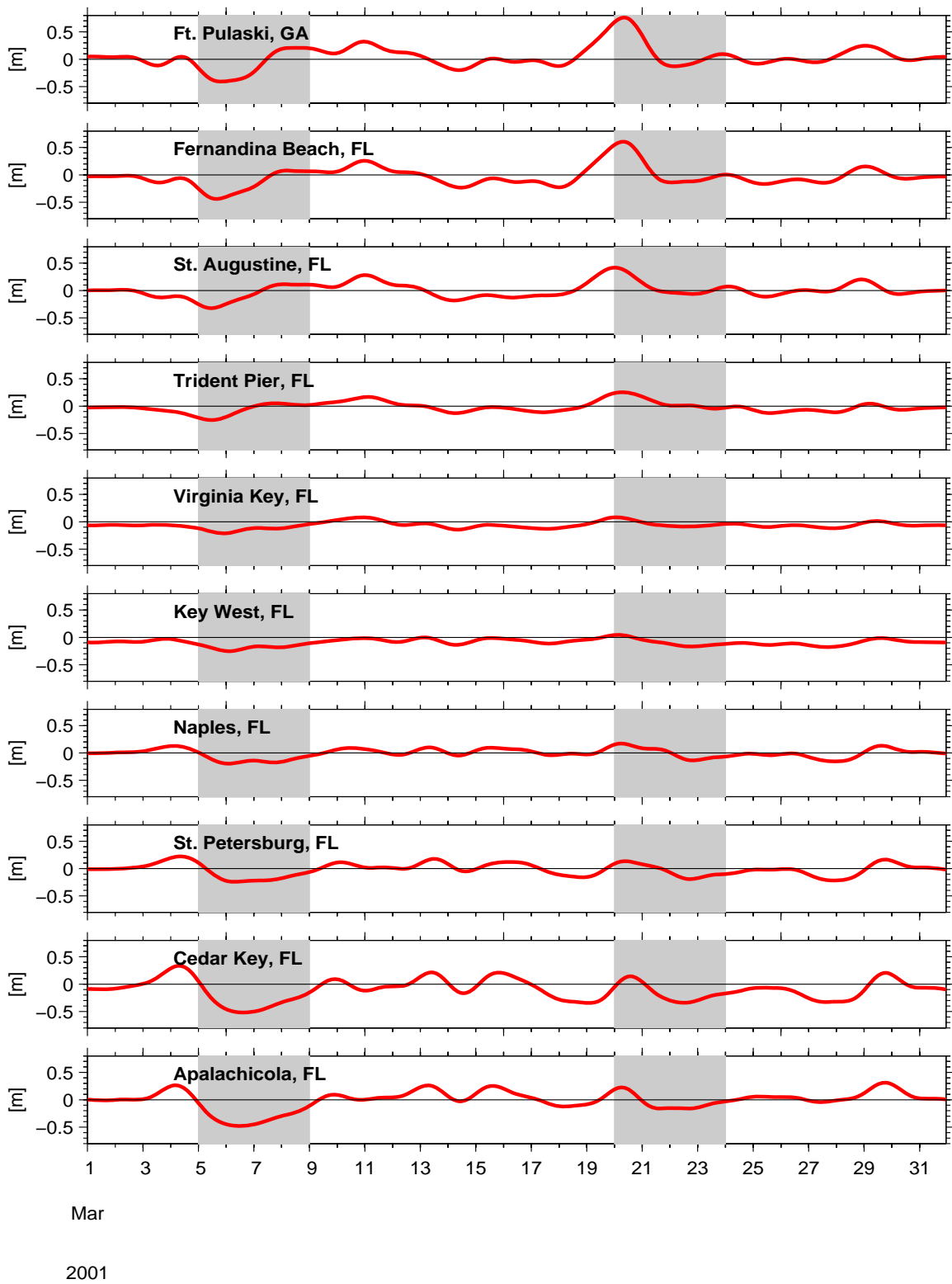
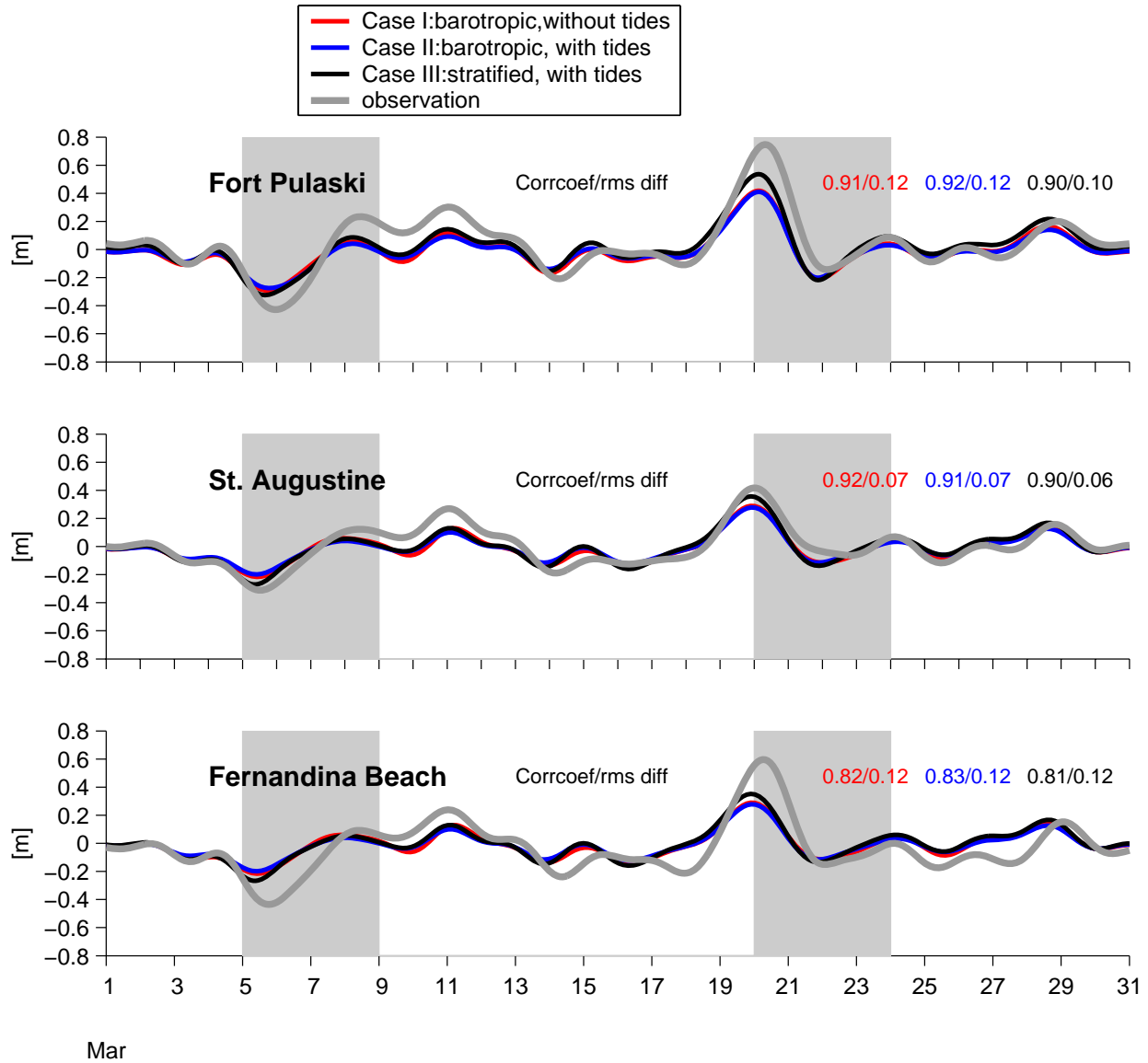


Figure 6. Time series of observed coastal sea levels during March, 2001, after adjustment for barometric pressure and 40-hr low-pass filtered. The shaded intervals indicate the storm passages.



2001

Figure 7. Comparison between observed and hindcast sea levels in the CGB domain. Cases I, II, III (see Table 3) and observations are in red, blue, black, and gray, respectively. All time series are 40-hr low-pass filtered. The number pair indicates the correlation coefficient and the *rms* difference (m) for each case. The shaded intervals indicate the storm passages.

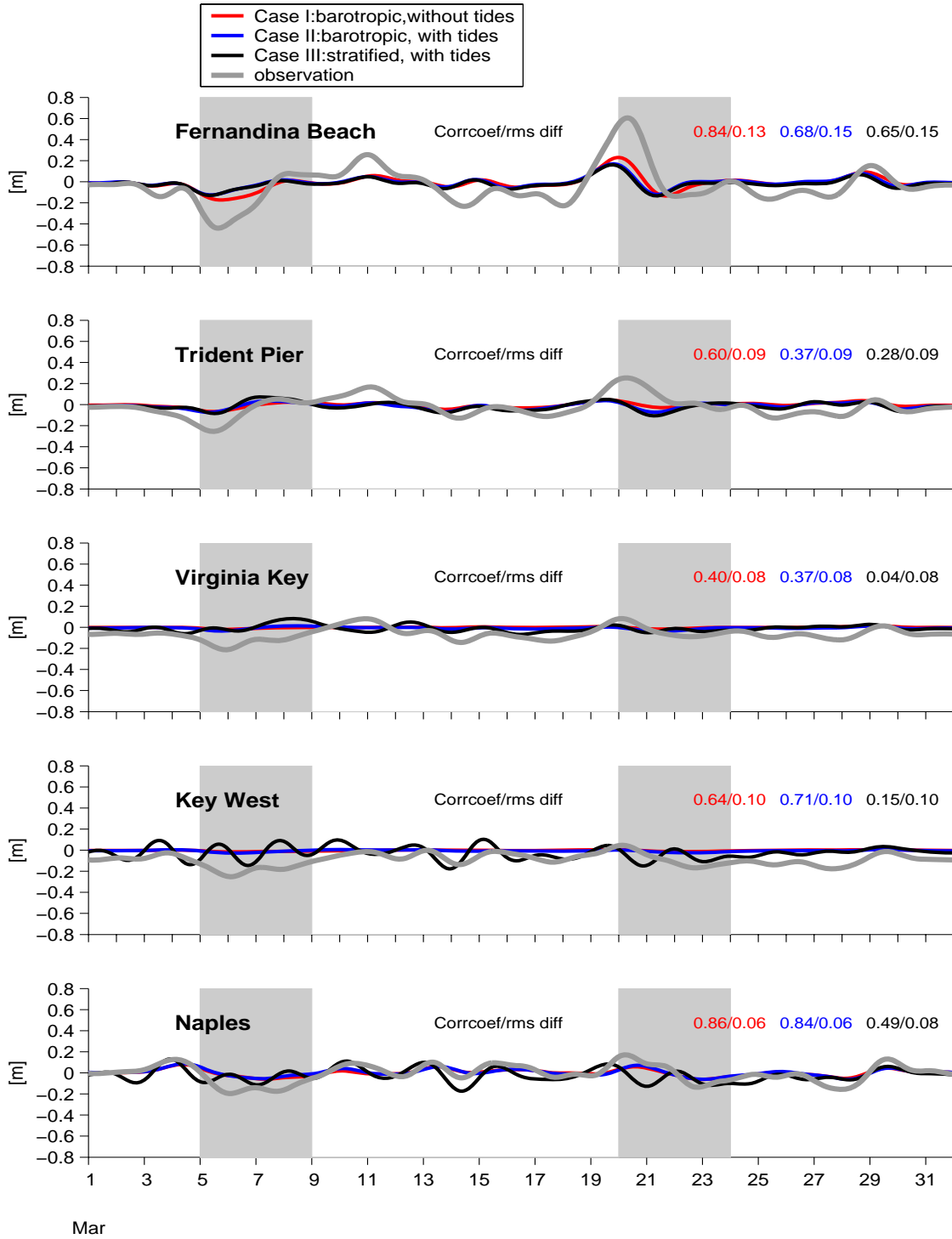
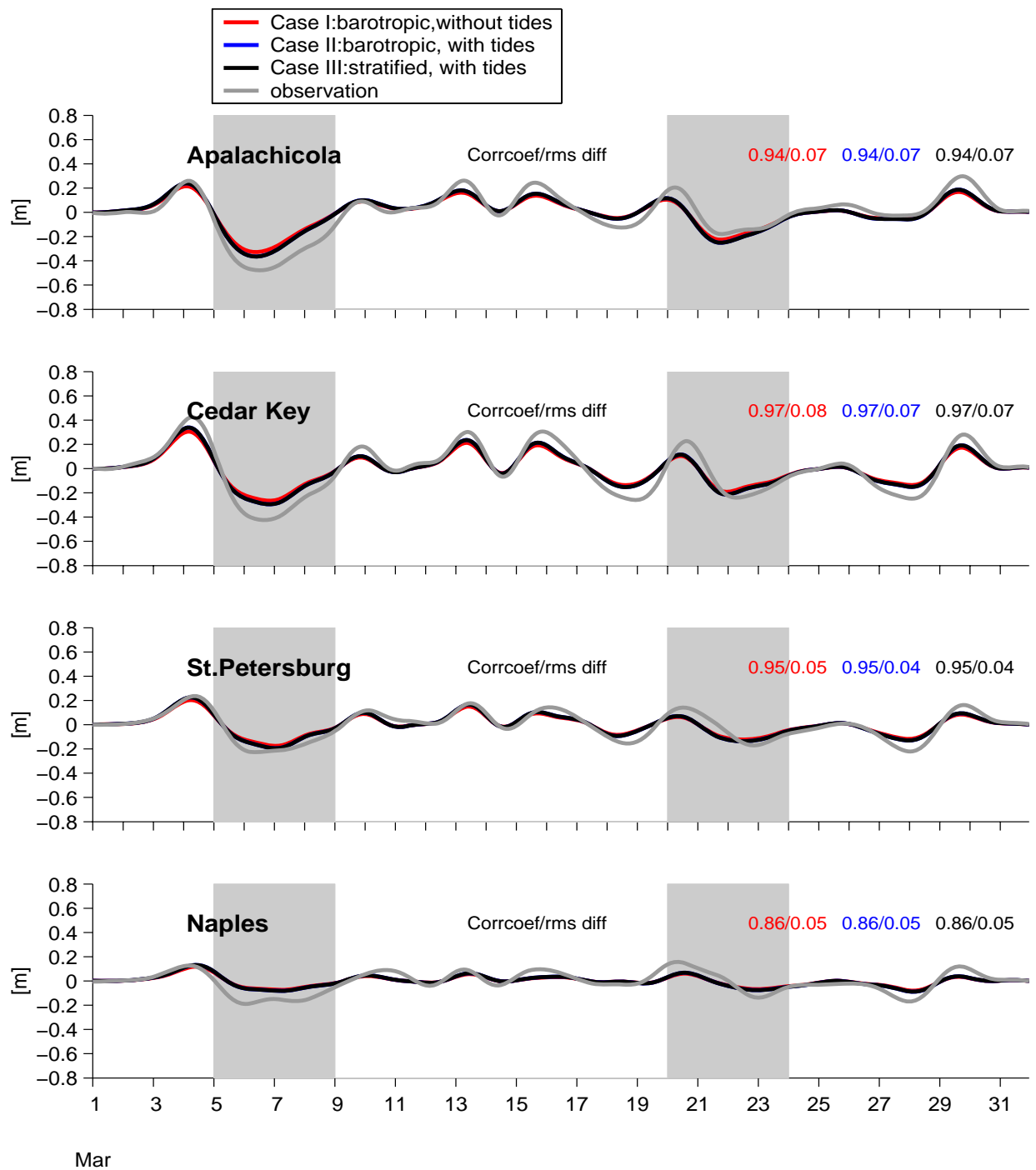
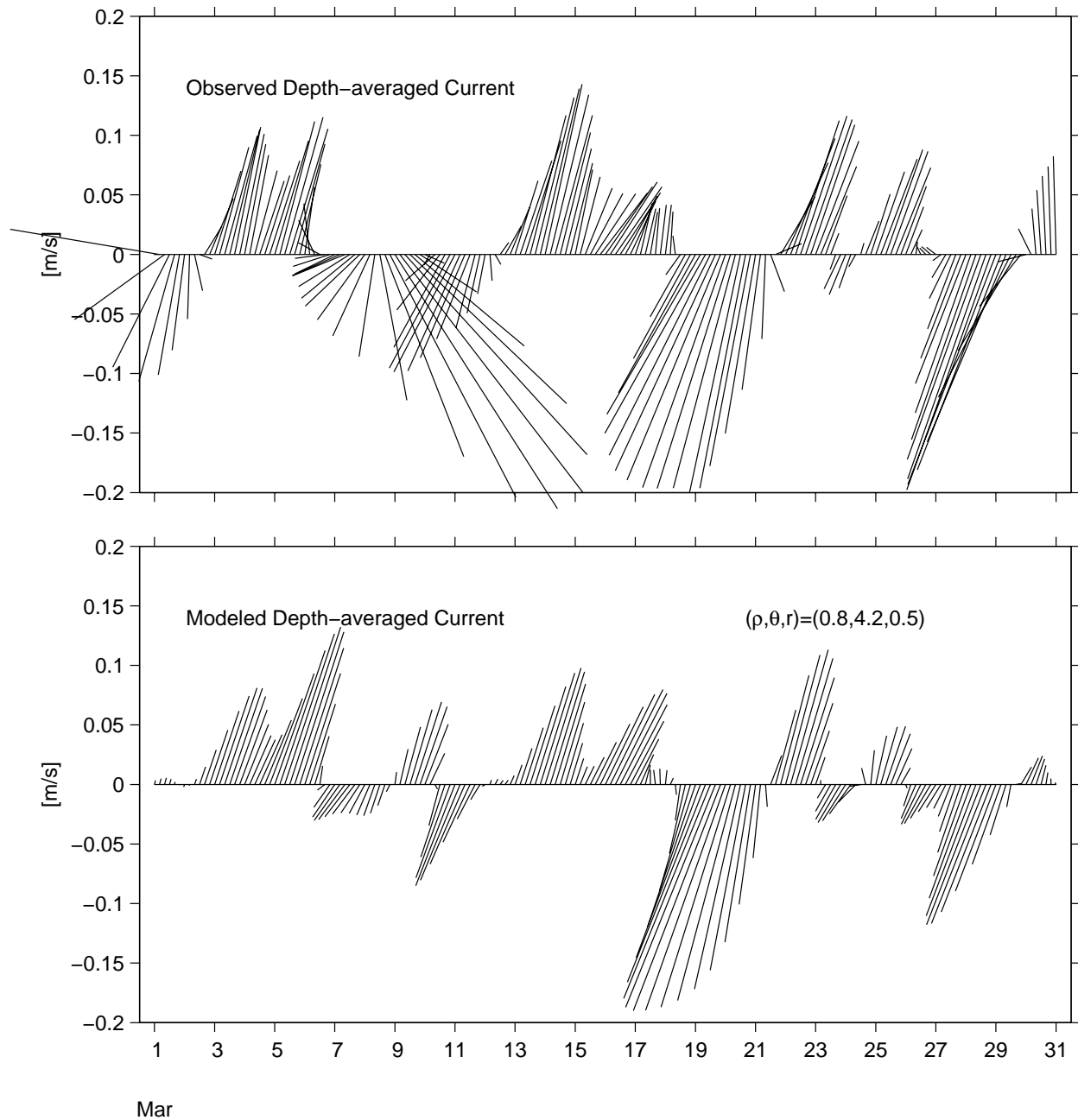


Figure 8. Comparison between observed and hindcast sea levels in the EFS domain. Cases I, II, III (see Table 3) and observations are in red, blue, black, and gray, respectively. All time series are 40-hr low-pass filtered. The number pair indicates the correlation coefficient and the *rms* difference (m) for each case. The shaded intervals indicate the storm passages.

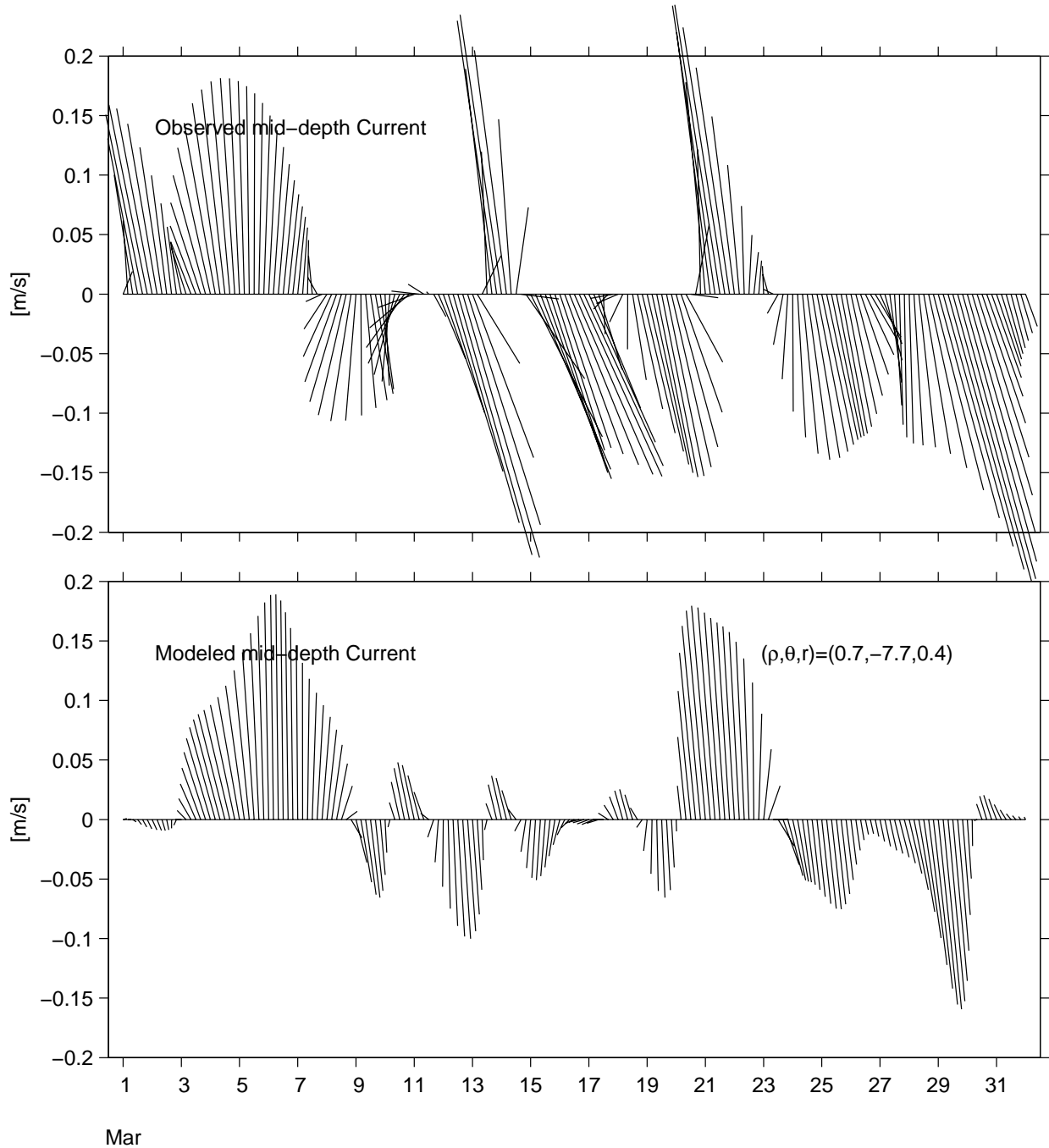


2001  
 Figure 9. Comparison between observed and hindcast sea levels in the WFS domain. Cases I, II, III and observations are in red, blue, black, and gray, respectively. All time series are 40-hr low-pass filtered. The number pair indicates the correlation coefficient and the *rms* difference (m) for each case. The shaded intervals indicate the storm passages.



2001

Figure 10. Comparison between observed and hindcast (Case III) depth-averaged currents at SAB Navy tower R2 at 25 m isobath. The model/data comparison is quantified by its complex correlation coefficient  $\rho$ , phase angle  $\theta$  (or angular deviation of the model vector from the data vector measured count-clockwise) in degrees, and regression coefficient  $r$ .



2001

Figure 11. Comparison between observed and hindcast (Case II) mid-depth currents at EFS Hawk Channel near Looe Key at 10 m isobath. Currents are rotated 90 degrees counter-clockwise, i.e., east is upward. The model/data comparison is quantified by its complex correlation coefficient  $\rho$ , phase angle  $\theta$  (or angular deviation of the model vector from the data vector measured count-clockwise) in degrees and regression coefficient  $r$ .

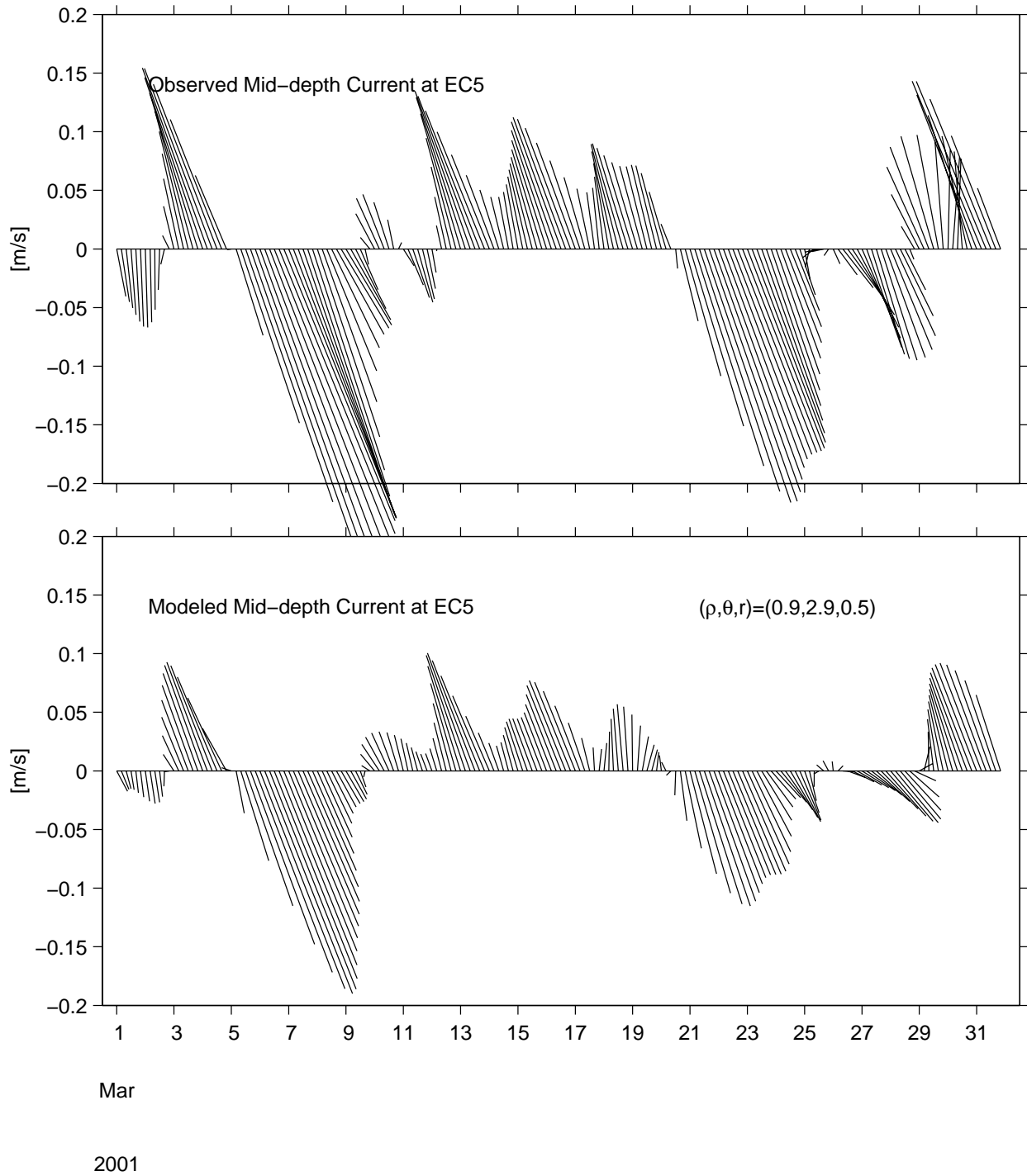


Figure 12. Comparison between observed and hindcast (Case III) mid-depth currents at WFS EC5 at 10 m isobath. The model/data comparison is quantified by its complex correlation coefficient  $\rho$ , phase angle  $\theta$  (or angular deviation of the model vector from the data vector measured count-clockwise) in degrees, and regression coefficient  $r$ .

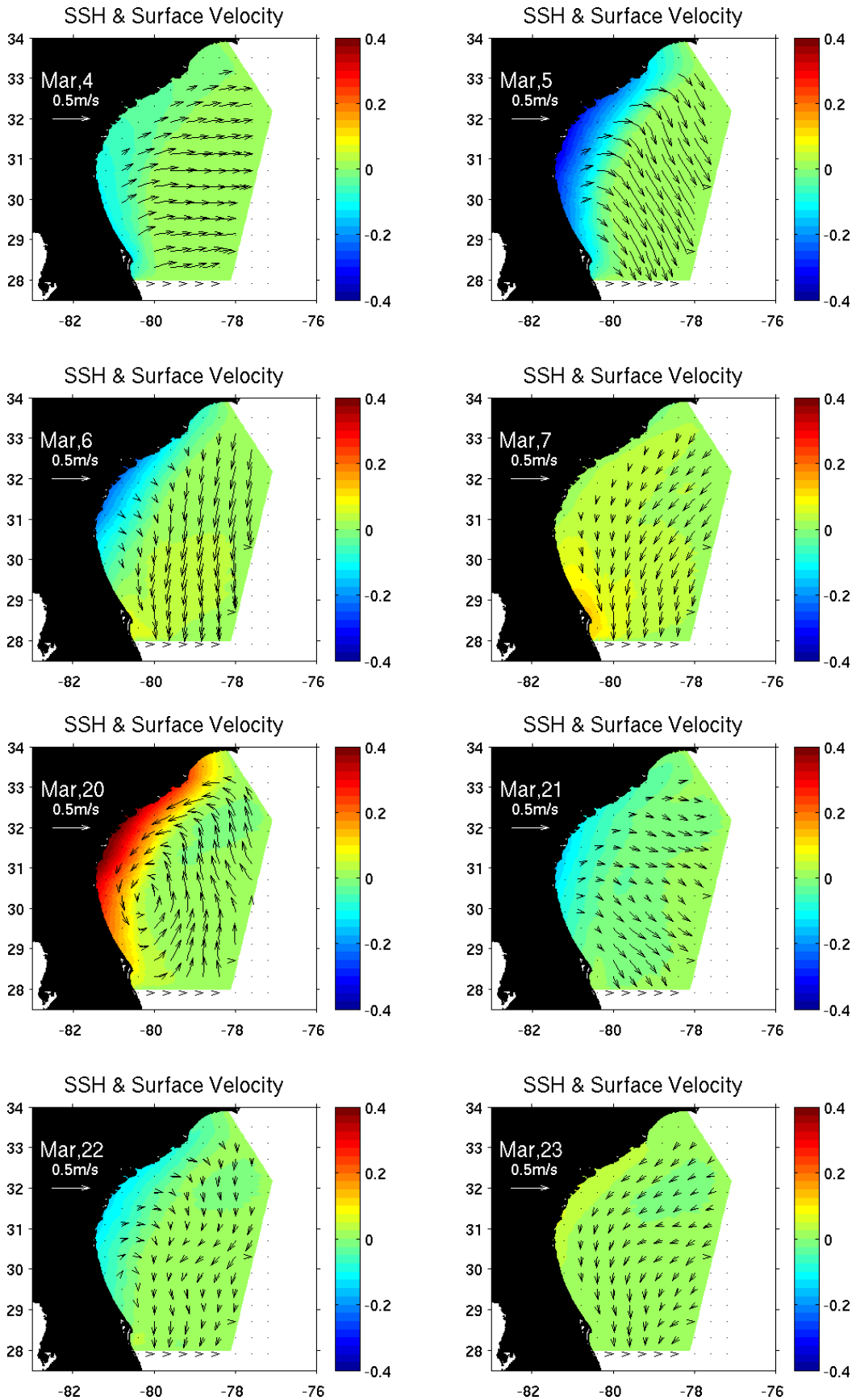


Figure 13. Snapshots of daily hindcast (UNC QUODDY Case I) surface current vectors and sea surface heights in color (m) during the first (upper four panels) and the second (lower four panels) storm passages in CGB.

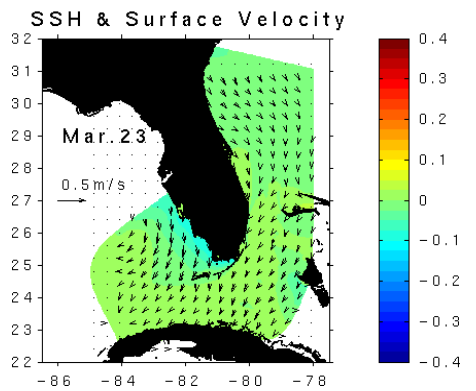
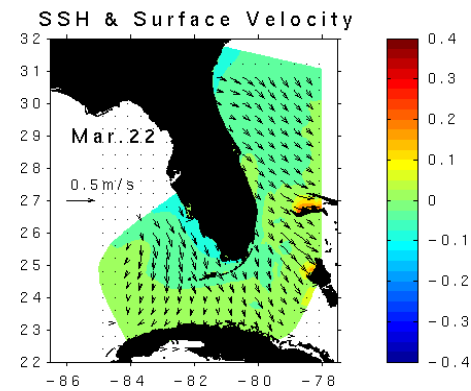
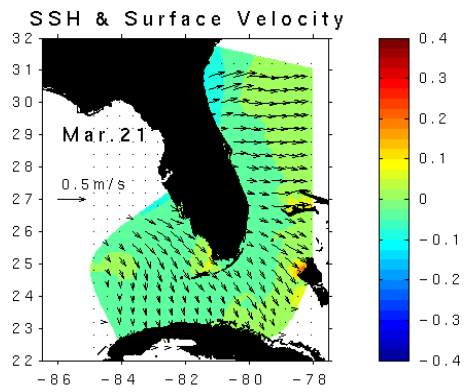
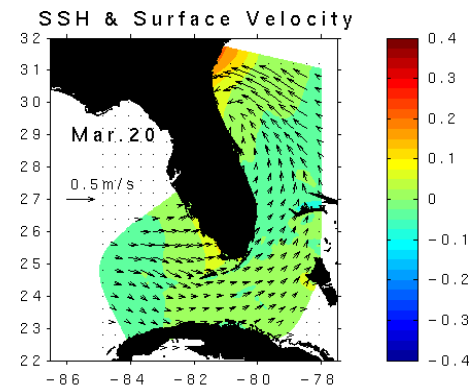
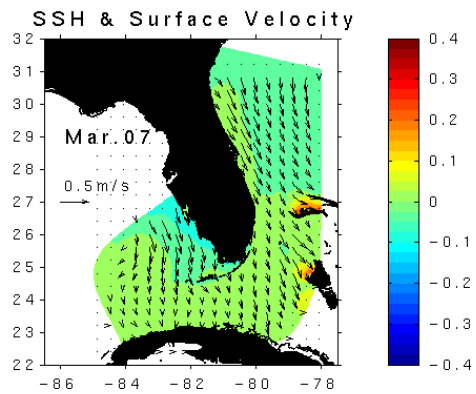
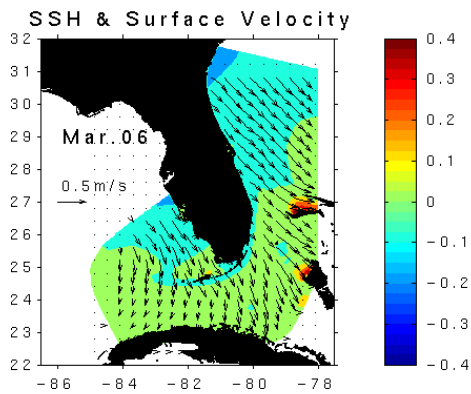
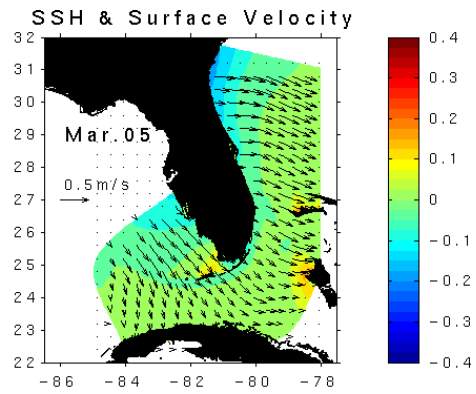
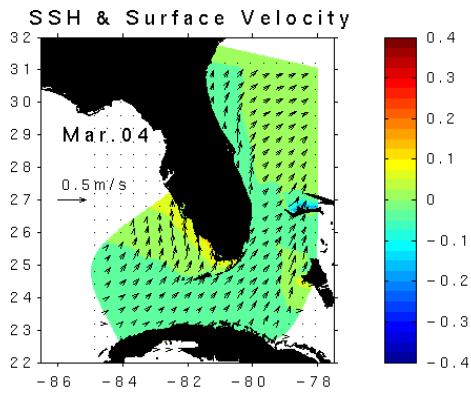


Figure 14. Snapshots of daily hindcast (UM POM Case I) surface current vectors and sea surface heights in color (m) during the first (upper four panels) and the second (lower four panels ) storm passages in EFS.

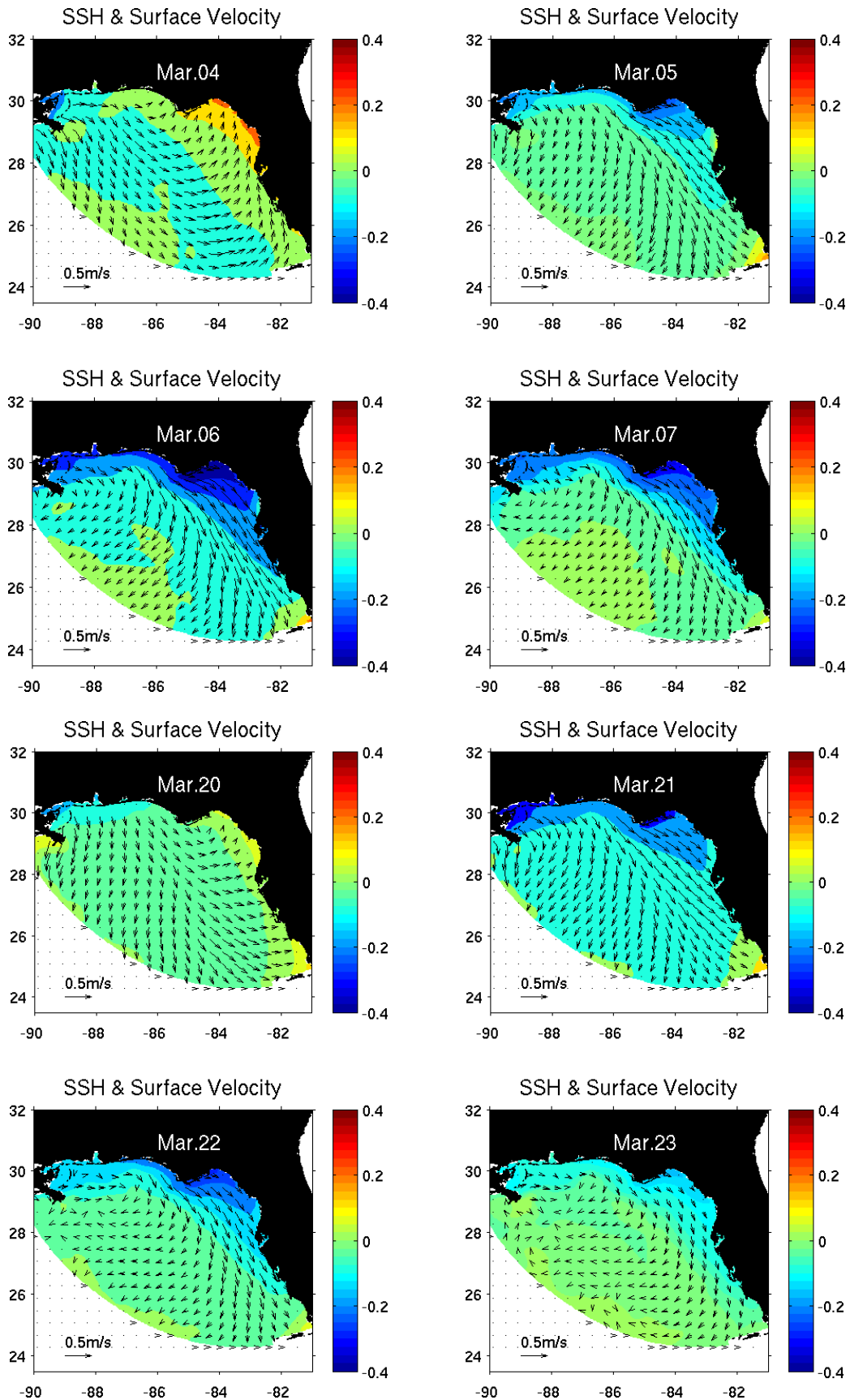


Figure 15. Snapshots of daily hindcast (USF POM Case I) surface current vectors and sea surface heights in color (m) during the first (upper four panels) and the second (lower four panels) storm passages in WFS.

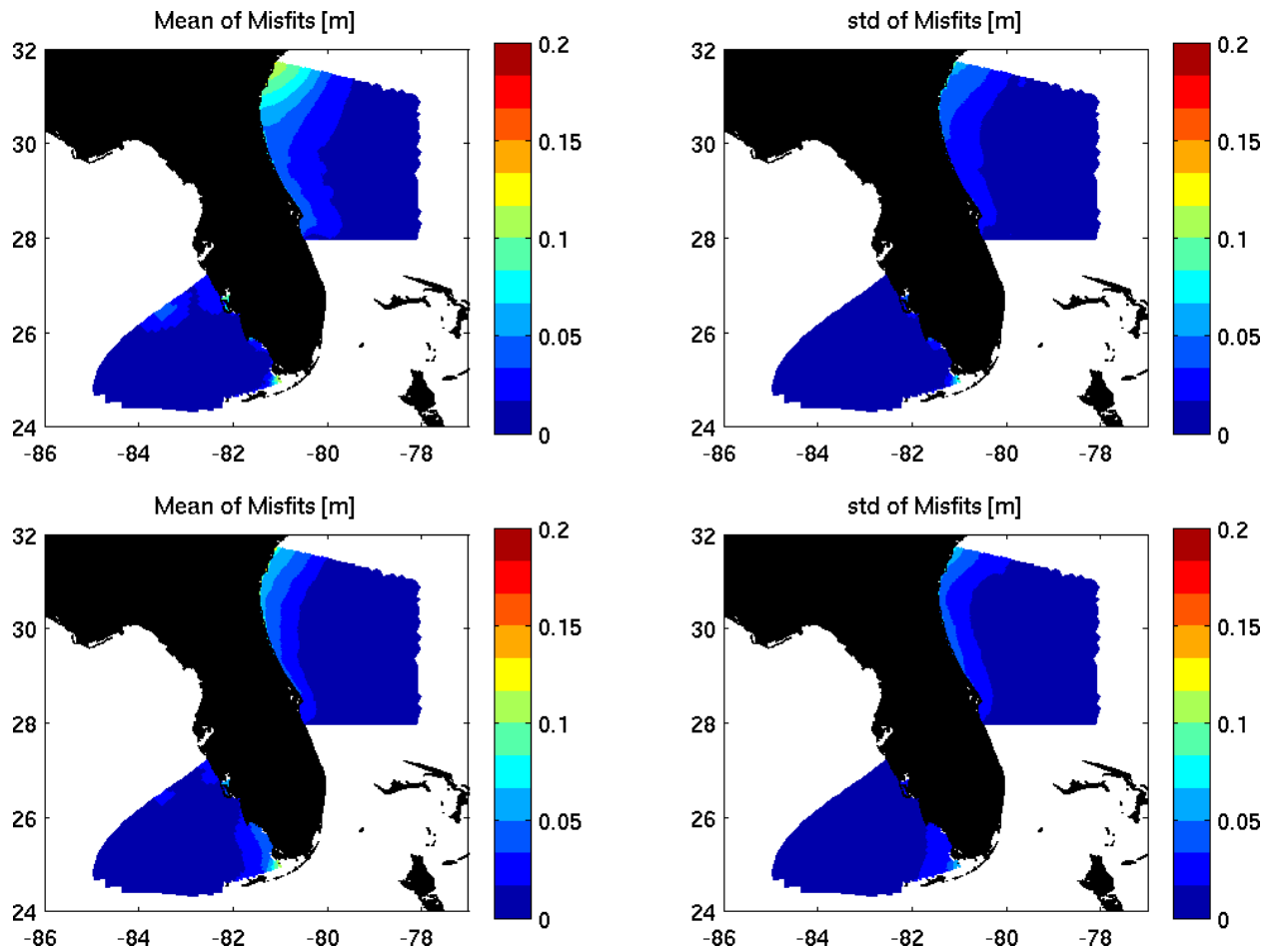


Figure 16. Mean and standard deviation maps of absolute hindcast (Case 1) sea level misfits (m) in overlapping regions between two adjacent sub-regions during the first (upper two panels) and the second (lower two panels) storm passages.